Large carrier-capture rate of Pb_I antisite in $CH_3NH_3PbI_3$ induced by heavy atoms and soft phonon modes

Jiqiang Li,[1,2] Hai-Feng Zhu,[1,2] Yue-Yu Zhang,[1,2] Zhen-Kun Yuan,[1,2] Shiyou Chen,[3,*] and Xin-Gao Gong[1,2,†]

[1]*Department of Physics, Key Laboratory for Computational Physical Science (Ministry of Education), State Key Laboratory of Surface Physics, Fudan University, Shanghai 200433, China*

[2]*Collaborative Innovation Center of Advanced Microstructures, Nanjing 210093, Jiangsu, China*

[3]*Key Laboratory of Polar Materials and Devices (Ministry of Education), East China Normal University, Shanghai 200241, China*

(Received 1 March 2017; revised manuscript received 18 July 2017; published 6 September 2017)

The Pb_I antisite was reported to be a possible deep-level recombination-center defect in $CH_3NH_3PbI_3$ solar cells with a concentration higher than $10^{15}\,cm^{-3}$ under I-poor conditions. However, whether it is really an effective nonradiative recombination center and limits the photovoltaic efficiency depends also on its cross sections for capturing the electron or hole carriers, which is difficult to determine in both experiment and theory. Here we use a recently developed method to overcome the high computational cost of electron-phonon coupling calculation and implement it in the standard first-principles code QUANTUM ESPRESSO so that we can calculate the carrier-capture cross sections effectively for the point defects in complicated semiconductors, such as $CH_3NH_3PbI_3$. The calculation showed that both the hole- and the electron-capture cross sections and capture rates of Pb_I are large relative to those of the point defects in conventional semiconductors, such as Si or GaP, which is attributed mainly to the heavy Pb-I atoms and the soft phonon modes in this Pb halide. Nonradiative recombination increases the thermal energy by exciting the phonons in the soft Pb-I lattice, whereas the contribution of the organic CH_3NH_3 group is negligible. Since Pb_I has a higher concentration under I-poor conditions, especially when the semiconductor is p-type, our results suggest that the minority-carrier lifetime and thus the photovoltaic efficiency should be very limited in p-type $CH_3NH_3PbI_3$ and p-type doping should be avoided for fabricating high-efficiency $CH_3NH_3PbI_3$ solar cells under I-poor conditions. Similar calculations can be used for studying the influence of various defects on the photovoltaic performance of other organic-inorganic hybrid and inorganic halide perovskites, shedding light on the design of high-efficiency solar cells.

DOI: 10.1103/PhysRevB.96.104103

I. INTRODUCTION

The organic-inorganic hybrid halide perovskite $CH_3NH_3PbI_3$ has drawn intensive attention as the light-absorbing material in solar cells for the rapid increase in its power conversion efficiency (PCE), low fabrication cost, and earth-abundant component elements [1–10]. One critical reason for the high PCE is that the lifetime of photogenerated carriers is in the range of $0.5-1\,\mu s$ with a carrier diffusion length of 2–8 μm in $CH_3NH_3PbI_3$ solar cells as shown by the various transport measurements [11–13]. The long carrier lifetime was attributed to the low concentration of the deep-level point defects that may act as the nonradiative recombination centers of electron-hole carriers [14–17]. This was considered as a unique and benign character of the Pb-I-based perovskite semiconductors with the lone-pair electronic states in the valence bands, in contrast with the situation in conventional photovoltaic semiconductors, such as Si, CdTe, or $Cu(In,Ga)Se_2$ which usually have deep-level recombination-center defects.

However, more recent studies by Buin and co-workers [18,19] showed that the Pb_I antisite (a Pb atom replaces an I atom) is a deep-level defect in $CH_3NH_3PbI_3$ and its concentration could be very high in $CH_3NH_3PbI_3$ samples grown under I-poor conditions, especially when the sample is p-type doped. If the Pb_I antisite is really an effective recombination center, the photovoltaic performance of $CH_3NH_3PbI_3$ samples grown under I-poor conditions will be very limited [18,19]. It should be noted that whether a defect acts as an effective recombination center depends not only on its transition energy levels in the band gap and its concentration, but also on its cross section for capturing the electron or hole carriers. Although the calculations by Buin and co-workers [18,19] showed that the Pb_I antisite has a deep level in the band gap and a high concentration in I-poor samples, its carrier-capture cross section so far is unknown. Therefore it is still an open question whether the Pb_I defect is an effective recombination center.

The accurate determination of the carrier-capture cross sections of defects is challenging for both the experimental measurement and the theoretical calculation. Experimentally, there is no efficient and direct method for measuring the carrier-capture cross sections or nonradiative recombination rate induced by point defects [20–22]. Usually the carrier lifetime was measured, but it is difficult to identify which defect dominates the nonradiative recombination process, especially for the organic-inorganic hybrid halides which have various defects in the lattice. Theoretically, in order to calculate the carrier-capture cross section accurately, we have to calculate the electron-phonon (el-ph) coupling effect around the defect first. Using the conventional finite difference method, at least $3N$ *ab initio* self-consistent field (SCF) calculations are required (where N is the number of atoms in the supercell with a defect), which is computationally very expensive for a large supercell (of 100–200 atoms usually). For $CH_3NH_3PbI_3$, an even larger number of atoms in the supercell

*Corresponding author: chensy@ee.ecnu.edu.cn
†Corresponding author: xggong@fudan.edu.cn

is required for calculating the properties of defects, making the calculation unaffordable. Recently Shi and Wang [23] proposed a novel algorithm to evaluate all the el-ph coupling matrix elements with merely two SCF calculations, reducing the computational cost considerably, and they calculated the carrier-capture cross sections for defects in GaN and GaP using this method for the first time [23,24]. Alternative *ab initio* methods had also been developed for studying the defect-induced nonradiative recombination rate in other simple semiconductors, such as Si [25], GaN [23,24,26,27], and CdTe [28]. Such a calculation for complicated semiconductors, such as $CH_3NH_3PbI_3$, is attempted here. Due to the lack of the accurate data, Agiorgousis *et al.* [29] had to make assumptions on the carrier-capture cross sections of defects in $CH_3NH_3PbI_3$ in order to predict the influence of various defects on the photovoltaic performance. If the cross section can be calculated accurately, the prediction could be much more quantitative and reliable.

In this paper, we have implemented the new algorithm developed by Shi and Wang [23] in the widely used first-principles simulation package QUANTUM ESPRESSO [30] to accelerate the expensive el-ph coupling calculation for the organic-inorganic hybrid semiconductors. By virtue of the static coupling formulism [24], we studied the nonradiative recombination induced by the Pb_I antisite in $CH_3NH_3PbI_3$. The capture cross sections as well as the corresponding capture rates were calculated, and a mode analysis was presented. The calculated capture cross sections of Pb_I defects are relatively large, and mode analysis shows that these large capture cross sections are attributed to the heavy atoms and the soft phonon modes in the Pb-I lattice. Our paper suggests that: (i) the Pb_I antisite is an effective recombination center and is detrimental to the photovoltaic performance in p-type $CH_3NH_3PbI_3$ grown under I-poor conditions, and (ii) I-poor conditions and p-type doping should be avoided in order to obtain a high PCE. Using this method we can predict the influence of various defects on the photovoltaic performance more accurately and guide the future development of high PCE solar cells through defect control.

This paper is organized as follows. The computational methodology is described briefly in Sec. II. We present the calculated results and discuss them in Sec. III. Finally, Sec. IV concludes the paper.

II. COMPUTATIONAL METHODOLOGY

A. Static coupling formalism

Static coupling formalism [24] is used to calculate the nonradiative recombination rate. The nonradiative decay probability is given by

$$W_{fi} = \frac{2\pi}{\hbar}\sum_m\sum_m p(i,m)\left|\sum_k \langle\psi_f|\frac{\partial H}{\partial Q_k}|\psi_i\rangle\langle\chi_n|\boldsymbol{Q}_k|\chi_m\rangle\right|^2 \times \delta(\Delta E + E_m - E_n), \quad (1)$$

where the indices i and f label the initial (before capturing a carrier) and final (after capturing a carrier) electronic states, respectively, m and n label the initial and final phonon states, respectively, and index k runs over all the phonon modes. $\Delta E = E_{i0} - E_{f0}$ is the electronic energy difference between the initial and the final states, and E_m and E_n are the phonon energies in the initial and final states, respectively. The probability that the system is in the initial phonon state m is $p(i,m)$. The el-ph coupling matrix elements are $\langle\psi_f|\frac{\partial H}{\partial Q_k}|\psi_i\rangle$ (hereinafter abbreviated as C^k_{fi}) and $\langle\chi_n|\boldsymbol{Q}_k|\chi_m\rangle$'s are the lattice transition matrix elements which can be evaluated using path-integral techniques and Gaussian integration [24,31–33]. In order to obtain the decay probability W_{fi} between the defect level and the valence-band maximum (VBM) or conduction-band minimum (CBM) levels, we need to calculate: (i) the relaxation of atomic configuration ΔR (the structure change caused by the carrier capture), (ii) the phonon frequencies $\{\omega_k\}$ (the phonon energies) and their mode vectors $\{e_k(R)\}$, (iii) the defect transition energy levels ΔE, and (iv) the el-ph coupling matrix elements C^k_{fi}.

With the decay probability W_{fi} calculated, we can compute the carrier-capture rate $B = W_{fi}V$, where V is the volume of the supercell. Then the carrier-capture cross section $\sigma = B/\langle v\rangle$, where $\langle v\rangle = \sqrt{3k_BT/m^*}$ is the thermal velocity which depends on the temperature T and the effective masses m^* of the electron or hole carriers. For $CH_3NH_3PbI_3$, the effective mass of the holes is $m^*_h = 0.25m_0$, and the effective mass of the electrons is $m^*_e = 0.19m_0$ [34].

Using static coupling formalism, we calculated the carrier-capture rate and cross section for the Pb_I antisite in a 384-atom supercell of tetragonal $CH_3NH_3PbI_3$ (the room-temperature β phase). The el-ph coupling matrix elements were calculated by our modified version of QUANTUM ESPRESSO [30] in which the accelerated algorithm [23] was implemented. The benchmark test and more calculation details are described in the Supplemental Material [35].

B. Accelerated algorithm for el-ph coupling calculation

The common form of the el-ph coupling matrix elements is $\langle\psi_f|\frac{\partial H}{\partial Q_k}|\psi_i\rangle = \sum_R \langle\psi_f|\frac{\partial H}{\partial R}\frac{\partial R}{\partial Q_k}|\psi_i\rangle = \sum_R \frac{e_R(k)}{\sqrt{M_R}}\langle\psi_f|\frac{\partial H}{\partial R}|\psi_i\rangle$, so the calculation of $\langle\psi_f|\frac{\partial H}{\partial R}|\psi_i\rangle$ is fundamental to the el-ph coupling calculation. In density functional theory (DFT), H is the SCF single-particle Hamiltonian. Some $3N$ SCF calculations are needed if the conventional finite difference method is employed. Here we adopted the accelerated algorithm proposed by Shi and Wang [23], and only two SCF calculations are necessary. The basic idea of this accelerated algorithm is introduced below.

In a conventional DFT calculation with a norm-conserving pseudopotential (NCPP), the single-particle Hamiltonian can be denoted by

$$H = -\frac{\hbar^2}{2}\sum_k \nabla^2 + V_{\text{tot}} + \sum_{I,nm}|\beta^I_n\rangle\langle\beta^I_m|, \quad (2)$$

where V_{tot} is the total local potential (containing the Hartree potential, the local part of the NCPP, and the exchange-correlation potential), $|\beta^I_n\rangle$ is the nonlocal part of the NCPP (the formalism is different for the ultrasoft pseudopotentials and has not been implemented in the present paper). I labels the ions, and the indices n and m indicate the angular momentum dependence. Apparently, the first term of the Hamiltonian

makes no contribution to el-ph coupling matrix elements, so,

$$\langle\psi_f|\frac{\partial H}{\partial R}|\psi_i\rangle = \langle\psi_f|\frac{\partial V_{\rm tot}}{\partial R}|\psi_i\rangle + \sum_{I,nm}\langle\psi_f|\frac{\partial}{\partial R}\left(|\beta_n^I\rangle\langle\beta_m^I|\right)|\psi_i\rangle. \quad (3)$$

The el-ph coupling matrix elements are divided into two parts and are calculated separately. The contribution from the total local potential can be written in the integral form

$$\langle\psi_f|\frac{\partial V_{\rm tot}}{\partial R}|\psi_i\rangle = \int {\rm Re}[\psi_f^*(r)\psi_i(r)]\frac{\partial V_{\rm tot}}{\partial R}dr = \int \rho_{fi}\frac{\partial V_{\rm tot}}{\partial R}dr. \quad (4)$$

If we replace the original charge density by the pseudocharge density $\rho_\lambda(r)$ [denoted as Eq. (5)] in SCF loops while keeping the extra charge density ρ_{fi} fixed, then the total energy can be given by Eq. (6),

$$\rho_\lambda(r) = \sum_k |\psi_k(r)|^2 + \lambda\rho_{fi}, \quad (5)$$

$$E[\psi,R,\lambda] = -\frac{\hbar^2}{2}\sum_k\langle\psi_k|\nabla^2|\psi_k\rangle + U[\rho_\lambda,R] + \sum_{k,I,nm}\langle\psi_k|\beta_n^I\rangle\langle\beta_m^I|\psi_k\rangle. \quad (6)$$

U is the total local potential energy (including the Hartree energy and the contribution from the local part of the NCPP and exchange-correlation energy), which is a functional of both pseudocharge density ρ_λ and atomic positions R. We denote the atomic force on the atom R as F_R and consider that $\langle\partial E/\partial\psi_k|\partial\psi_k/dX\rangle = 0$ (where X can be λ and R) [36], then we have [23]

$$\begin{aligned}\frac{dF_R}{d\lambda} &= -\frac{d}{d\lambda}\frac{dE[\psi,R,\lambda]}{dR} = -\frac{d}{dR}\frac{dE[\psi,R,\lambda]}{d\lambda}\\ &= -\frac{d}{dR}\left\{\sum_k\left\langle\frac{\partial E}{\partial\psi_k}\middle|\frac{\partial\psi_k}{d\lambda}\right\rangle + \frac{\partial}{\partial\lambda}E\right\}\\ &= -\int\frac{d}{dR}\left\{\frac{\partial U[\rho_\lambda,R]}{\partial\rho_\lambda}\frac{\partial\rho_\lambda}{\partial\lambda}\right\}dr\\ &= -\int\frac{d}{dR}\{V_{\rm tot}\rho_{fi}(r)\}dr\\ &= -\int\rho_{fi}\frac{\partial V_{\rm tot}}{\partial R}dr\\ &= -\langle\psi_f|\frac{\partial V_{\rm tot}}{\partial R}|\psi_i\rangle. \end{aligned} \quad (7)$$

Note that all the atomic forces F_R can be calculated by virtue of Hellman-Feynman theory in the conventional DFT calculations [30,37],

$$F_R = -\int\rho_\lambda\frac{\partial V_{\rm ion}}{\partial R}dr - \sum_{kI,nm}2{\rm Re}\left[\left\langle\psi_k\middle|\frac{d\beta_n^I}{dR}\right\rangle\langle\beta_m^I|\psi_k\rangle\right]. \quad (8)$$

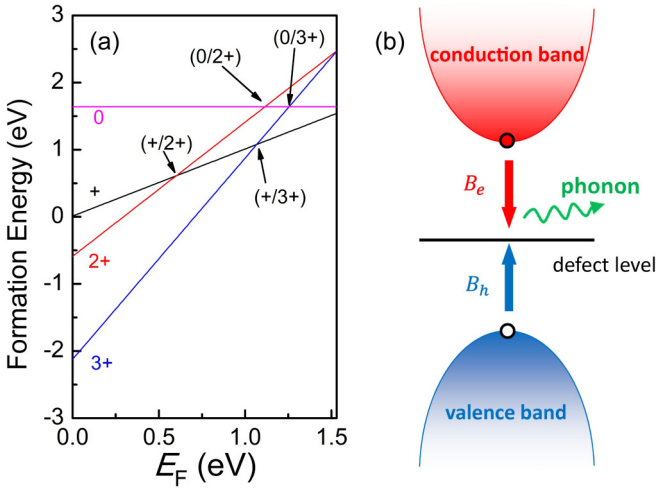

FIG. 1. (a) The calculated formation energy of a Pb_I defect at different charge states. E_F is the Fermi energy referenced to the VBM level. (b) Schematic of the nonradiative carrier capture of the electron or hole through the defect level in the band gap.

With two SCF calculations (one $\lambda = 0$ and another $\lambda =$ small), we can obtain the contribution from the total local potential.

Since the contribution from the nonlocal part of the NCPP is independent of the SCF calculation [30,37], its calculation can be included in the standard SCF calculation (with $\lambda = 0$). Therefore the two parts in Eq. (3) can be obtained with two SCF calculations.

III. RESULTS AND DISCUSSION

In order to study the nonradiative recombination induced by Pb_I, we need to know the different charge states at which the defect can capture electron or hole carriers and thus induce a nonradiative recombination process. Pb_I can be stable in $CH_3NH_3PbI_3$ at four charge states, 0 (neutral, not ionized), +1, +2, and +3. Their calculated formation energies as a function of the Fermi energy are shown in Fig. 1(a). Transitions among these charge states produce four transition energy levels in the band gap, i.e., the (+/2+), (+/3+), (0/2+), and (0/3+) levels, which may act as recombination-center levels according to the Shockley-Read-Hall theory [38,39]. These deep levels can capture hole carriers from the VBM state or electron carriers from the CBM state as shown in Fig. 1(b). For example, the +1 charged Pb_I can capture a hole from the VBM and transit into the +2 charged state, inducing a (+/2+) transition, and the +2 charged Pb_I can capture an electron from the CBM and transit into the +1 charged state, inducing a (2 + /+) transition.

Since the possibility of a point defect capturing two or more holes (electrons) simultaneously is usually very small due to the Coulomb repulsion between two holes (electrons), the nonradiative recombination through the (0/2+), (+/3+), and (0/3+) levels can be neglected, and thus we only need to consider the recombination through the (+/2+) level. The formation energies of +2 and +1 charged Pb_I are both lower than 1.0 eV when the Fermi level is below 0.75 eV, meaning that their concentration can be high in p-type samples and

their influence on the nonradiative recombination cannot be neglected, so in the following discussion we will focus on the influence of the +2 and +1 charged Pb_I, although their concentrations are lower than that of +3 charged Pb_I when the $CH_3NH_3PbI_3$ sample is doped into p-type. The calculated (+/2+) transition energy level is located at 0.6 eV above the VBM, namely, 0.93 eV below the CBM. If the $CH_3NH_3PbI_3$ sample is doped into n-type with a high concentration of electron carriers, and thus the Fermi level is located close to the CBM (1.53 eV), more Pb_I antisites are in the +1 charged state than in the +2 charged state, and they can capture a hole (the minority carrier in the n-type sample) from the VBM and have a transition into the +2 charge state, leading to a nonradiative recombination process. Therefore the hole-capture rate B_h determines whether the Pb_I^+ defect is an effective recombination center in n-type $CH_3NH_3PbI_3$. If the $CH_3NH_3PbI_3$ sample is doped into p-type with a high concentration of hole carriers and thus the Fermi level is located close to the VBM (0), more Pb_I antisites are in the +2 charged state than in the +1 charged state, and they can capture an electron (the minority carrier in the p-type sample) from the CBM and have a transition into the +1 charge state, leading to a nonradiative recombination process. Therefore the electron-capture rate B_e determines whether the Pb_I^{2+} defect is an effective recombination center in p-type $CH_3NH_3PbI_3$.

The calculated hole-capture rate of Pb_I^+ in $CH_3NH_3PbI_3$ is $B_h = 4.1 \times 10^{-7}\,\mathrm{cm}^3/\mathrm{s}$, and the corresponding hole-capture cross section is $\sigma_h = 1.8 \times 10^{-14}\,\mathrm{cm}^2$ at 300 K. The hole-capture cross section of Pb_I^+ is relatively large compared to those of the point defects or dopants in conventional semiconductors, e.g., the Au impurity in Si ($1 \times 10^{-15}\,\mathrm{cm}^2$) [40] and the (Zn,O) impurity in GaP ($< 5 \times 10^{-17}\,\mathrm{cm}^2$) [41]. Typical experimental values of capture cross sections for defects in a wide variety of semiconductors (such as GaAs and GaP) [41,42] vary from 10^{-21} to $10^{-13}\,\mathrm{cm}^2$, which puts our calculated hole-capture cross section σ_h close to the upper limit of these experimental values. The large cross section means that the lifetime of the minority carrier (hole) is limited to only $\tau = \frac{1}{B_h N_D} = 2.4\,\mathrm{ns}$ if the concentration of Pb_I^+ is $N_D = 1 \times 10^{15}\,\mathrm{cm}^{-3}$ in the n-type $CH_3NH_3PbI_3$. In order to achieve a long carrier lifetime around 1 μs, the concentration of Pb_I^+ should be lower than $N_D = \frac{1}{B_h \tau} = 2.4 \times 10^{12}\,\mathrm{cm}^{-3}$ in n-type $CH_3NH_3PbI_3$.

The calculated electron-capture rate is $B_e = 2.8 \times 10^{-9}\,\mathrm{cm}^3/\mathrm{s}$, and the corresponding electron-capture cross section is $\sigma_e = 1.0 \times 10^{-16}\,\mathrm{cm}^2$ at 300 K. The electron-capture cross section is also large compared to those in conventional semiconductors, e.g., the In impurity in Si ($4 \times 10^{-17}\,\mathrm{cm}^2$) [43] and the Zn impurity in Si ($1 \times 10^{-19}\,\mathrm{cm}^2$) [41]. With such a large electron-capture rate, the electron lifetime should be limited to lower than 0.36 μs if the concentration of Pb_I^{2+} is higher than $1 \times 10^{15}\,\mathrm{cm}^{-3}$ in p-type $CH_3NH_3PbI_3$, and the concentration of Pb_I^{2+} should be lower than $3.6 \times 10^{14}\,\mathrm{cm}^{-3}$ in order to obtain a carrier lifetime longer than 1 μs.

Both the electron- and the hole-capture rates (and the cross sections) increase as the temperature T increases. In Fig. 2 the calculated B_h's and B_e's are plotted as a function of the transition energy-level ΔE at different temperatures. At higher temperatures, B_h and B_e are obviously larger because

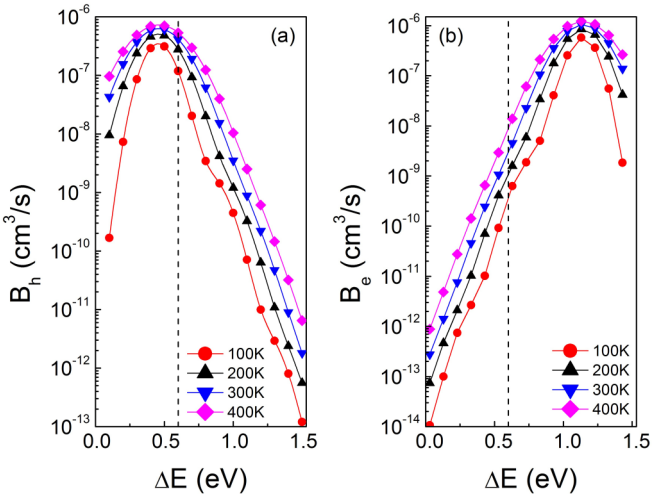

FIG. 2. The dependence of (a) hole- and (b) electron-capture rates of the Pb_I defect on the transition levels at different temperatures.

the nonradiative recombination (the electron capture or the hole capture by the defects in the lattice) is fundamentally a process in which the electron or hole jumps down from the high-energy state to the low-energy state and meanwhile the phonons are excited with the electronic energy converted into the thermal energy. At higher temperatures, there are more excited phonons, which can facilitate the energy-conversion process and thus increase the capture rate.

In Fig. 2 we also can see that there is a peak in the dependence of B_h and B_e on the Pb_I (+/2+) transition energy-level ΔE. To understand the peak we plot the configuration coordinate diagram for the carrier-capture process in Fig. 3. Under the harmonic approximation and considering only the single vibrational mode, the energies of the initial and final

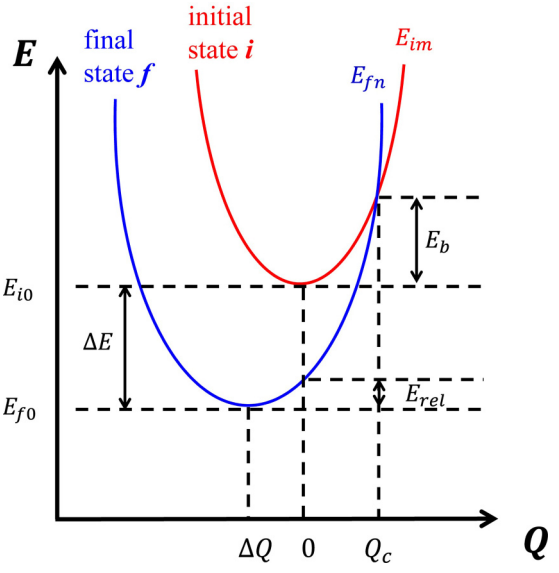

FIG. 3. The schematic coordinate diagram for the electron-capture or hole-capture process. Q is an appropriately chosen configuration coordinate.

states as a function of the configuration coordinate are given by [44]

$$E_{im} = E_{i0} + \tfrac{1}{2}\omega_0^2 Q^2, \tag{9}$$

$$E_{fn} = E_{f0} + \tfrac{1}{2}\omega_0^2 (Q - \Delta Q)^2, \tag{10}$$

where E_{i0} and E_{f0} are the equilibrium energies of the two states, Q is the configuration coordinate, ΔQ is the change of equilibrium configuration coordinates from the initial state to the final state, and ω_0 is the corresponding frequency. The energy difference $E_{i0} - E_{f0}$ at the equilibrium states is equal to the $(+/2+)$ transition energy-level ΔE of Pb_I. The transition (electron or hole capture) occurs when the energy curves of the two states cross at $Q = Q_c$, where $E_{im} = E_{fn}$. Therefore we can determine that the configuration coordinate Q_c of the cross point is

$$Q_c = \frac{E_{\rm rel}^0 - \Delta E}{\omega_0^2 \Delta Q}, \tag{11}$$

in which $E_{\rm rel}^0 = \frac{1}{2}\omega_0^2 \Delta Q^2$ is defined as the lattice relaxation energy (the energy change caused by the equilibrium configuration coordinate difference between the initial and the final states) [45]. There is an energy barrier for this transition [44],

$$E_b^0 = \frac{1}{2}\omega_0^2 Q_c^2 = \frac{\left(E_{\rm rel}^0 - \Delta E\right)^2}{4E_{\rm rel}^0}. \tag{12}$$

When it is generalized to the case of multivibrational modes, the energy barrier is given by [44,46]

$$E_b = \frac{(E_{\rm rel} - \Delta E)^2}{4E_{\rm rel}}, \tag{13}$$

where $E_{\rm rel} = \sum_k \frac{1}{2}\omega_k^2 \Delta Q_k^2$. Kubo and Toyozawa [46] pointed out that the nonradiative transition is a typical temperature-activated process and occurs at the cross point. Alkauskas *et al.* [26] reported that, at high temperatures, the dependence of the capture rate on the energy barrier and temperature could be fitted to a function,

$$B = B_0 + B_1 \exp(-E_b/k_B T), \tag{14}$$

with a temperature-independent part and a temperature-activated part. When the lattice relaxation energy just compensates for the pure electronic energy difference, i.e., $\Delta E = E_{\rm rel}$, the cross point is just at the equilibrium configuration of the initial state, there will be no energy barrier for the carrier-capture process, i.e., $E_b = 0$, leading to a peak of the carrier-capture rate (transition rate). When ΔE deviates from $E_{\rm rel}$, the energy barrier E_b increases and becomes positive, and the carrier-capture rate decreases exponentially with $(\Delta E - E_{\rm rel})^2$, which is consistent with our calculated results in Fig. 2.

Our calculated $E_{\rm rel}$ for the hole-capture process is $E_{\rm rel} = 0.46$ eV. Since the $(+/2+)$ transition energy-level ΔE of Pb_I is 0.6 eV above the VBM (as shown by the dashed line in Fig. 2), very close to $E_{\rm rel}$, leading to a small energy barrier $E_b^h = 0.01$ eV, the calculated hole-capture rate B_h is close to its maximum on the order of 10^{-7} cm^3/s. In contrast, the calculated electron-capture rate B_e is two orders of magnitude smaller than B_h because the calculated $E_{\rm rel} = 0.39$ eV for the electron-capture process and thus B_e approaches its maximum when ΔE is 0.39 eV below the CBM. However, the calculated ΔE is 0.6 eV above the VBM (0.93 eV below the CBM), leading to a much higher-energy barrier $E_b^e = 0.19$ eV, so B_e is much smaller than its maximum as well as B_h.

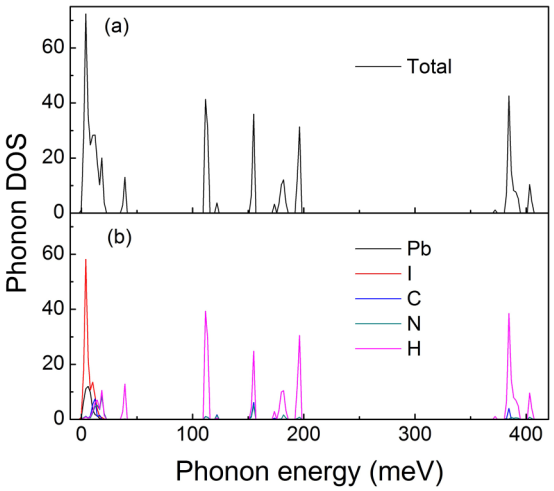

FIG. 4. (a) Total and (b) projected phonon DOS of the 384-atom $CH_3NH_3PbI_3$ supercell with a Pb_I^+ defect.

As mentioned above, the calculated carrier-capture rates (cross sections) of the Pb_I $(+/2+)$ level are large compared to those of the defect or dopant levels in conventional semiconductors, such as Si. To reveal the microscopic origin, we now will analyze the factors at the atomic and electronic levels that contribute to the large carrier-capture cross sections. Since the nonradiative carrier capture occurs via the multiphonon emission [23,42], a clear understanding of the lattice dynamics of $CH_3NH_3PbI_3$ is necessary and fundamental. The calculated phonon density of states (DOS) of the supercell with a Pb_I^+ defect is shown in Fig. 4. The phonon energies (frequencies) vary over a very wide range from 0 to 400 meV, which originates from the large differences between the atomic masses (thus different bond strengths) in this organic-inorganic hybrid material system. The projections of the phonon DOS on different component elements show that the phonon modes contributed by the heavy Pb and I atoms are located mainly in the low-energy region (below 30 meV), whereas the light atoms including H, C, and N contribute mainly to the high-frequency phonon modes. The case of the supercell with a Pb_I^{2+} defect is similar.

To show which phonons contribute more to the carrier-capture process, we plotted the hole-capture and electron-capture rates projected on the phonon modes in different energy ranges as shown in Figs. 5(c) and 5(f). Interestingly the contribution of the low-frequency (soft) phonons is obviously dominant, and the contribution of the high-frequency phonons is negligible, indicating clearly that the vibrations in the heavy Pb-I lattice are responsible for the large carrier-capture rates whereas the CH_3NH_3 organic group does not play an important or direct role in the carrier-capture process. The large CH_3NH_3 organic cation groups increase the lattice constant of $CH_3NH_3PbI_3$ significantly, which weakens the Pb-I bonds and

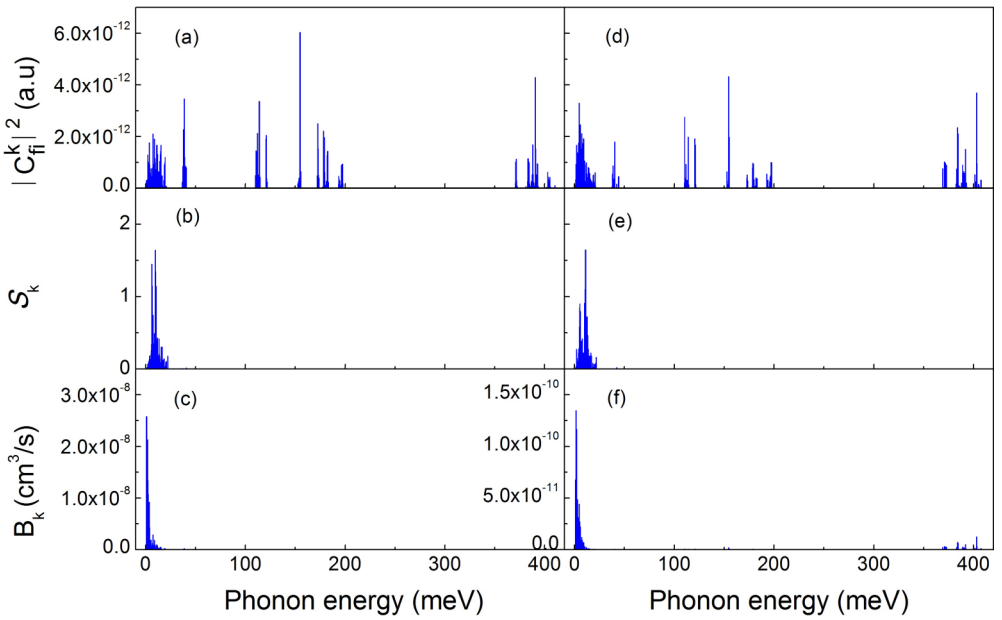

FIG. 5. The contribution of different phonon modes to the (a) and (d) squared norms of the el-ph coupling matrix elements $|C_{fi}^k|^2$, (b) and (e) Huang-Rhys factors S_k, (c) and (f) projected hole-capture and electron-capture rates at 300 K. The left column is for the supercell with a Pb_I^+ antisite, and the right column is for the supercell with a Pb_I^{2+} antisite.

makes the phonons softer, but their vibrations are not directly involved in the carrier-capture process.

To understand why the soft Pb-I phonons dominate the carrier-capture process (a phonon-assisted electronic transition from the initial state to the final state) in $CH_3NH_3PbI_3$, we plotted the el-ph coupling matrix elements for different phonon modes as shown in Figs. 5(a) and 5(d). For the hole-capture process, the initial electronic state is the VBM state, and the final state is the defect-level state, whereas for the electron-capture process, the initial electronic state is the CBM state, and the final state is the defect-level state. The initial state and the final state are coupled by the all the phonon modes as described quantitatively by the el-ph coupling matrix elements C_{fi}^k. Our calculations showed that C_{fi}^k's are large for both the low-frequency and the high-frequency phonon modes, so they all are the promoting modes that couple the two electronic states very efficiently. As a result, both the heavy inorganic atoms and the organic groups can play an important role in the el-ph coupling and assist the carrier-capture process, so we cannot explain why the soft Pb-I phonons dominate the carrier-capture process merely according to the calculated el-ph coupling matrix elements.

Although both the low-frequency and the high-frequency phonon modes can assist the carrier-capture process efficiently, the Huang-Rhys factors [47] of the low-frequency Pb-I phonons are much larger than those of the high-frequency phonons as shown in Figs. 5(b) and 5(e). The Huang-Rhys factor S_k, as defined by $S_k = \frac{\omega_k}{2\hbar}\Delta Q_k^2$, characterizes the average number of excited phonons for the kth normal mode in the carrier-capture process [48]. As mentioned above, the electronic energy is converted into the thermal energy stored in the phonons during the carrier-capture process. The calculated S_k shows that more low-frequency Pb-I phonons are excited to store the thermal energy, whereas the contribution of the high-frequency CH_3NH_3 phonon modes is negligible. This is because the lattice relaxation (ΔQ_k) caused by the carrier-capture is accommodated mainly by the soft Pb-I lattice around the Pb_I antisite whereas the structural change (such as the bond length change) in the CH_3NH_3 organic group is extremely small. In this way we can understand why the soft phonon modes of the heavy Pb and I atoms dominate the nonradiative carrier-capture processes and lead to the large B_h and B_e.

The large carrier-capture rates of Pb_I indicate that the carrier lifetime will be limited if its concentration is high. With the calculated formation energy (concentration) of Pb_I at different charge states as a function of the growth conditions (from I-poor to I-rich) and Fermi energy (from 0 at the VBM to 1.53 eV at the CBM) [18], we can predict the maximum lifetime of the minority carrier limited by Pb_I. In Fig. 6 we show the calculated dependence of the maximum lifetime of the minority hole (a) and electron (b) carrier on the growth conditions and Fermi energy. The label I-rich means the highest chemical potential (I-poor means the lowest chemical potential) that satisfies all these conditions, stabilizing the $CH_3NH_3PbI_3$ compound and meanwhile not causing the formation of any other secondary compounds, such as PbI_2 or CH_3NH_3I.

Due to the increase in the Pb_I concentration, the maximum lifetime decreases exponentially as the growth conditions change from I-rich to I-poor and as conductivity changes from n-type to p-type. Under I-rich conditions, the effect of Pb_I is negligible, and both the electron and the hole lifetimes can be very long. However, under I-poor conditions, the detrimental effect of Pb_I becomes much more obvious, i.e., the maximum electron and hole lifetimes can be longer than 1 μs if the sample is n-type with the Fermi energy close to the CBM level, but they are limited to less than 10^{-12} s if the sample is doped into p-type (the Fermi energy is close to the VBM level). These results show definitely that Pb_I is an effective nonradiative recombination center in p-type and I-poor $CH_3NH_3PbI_3$.

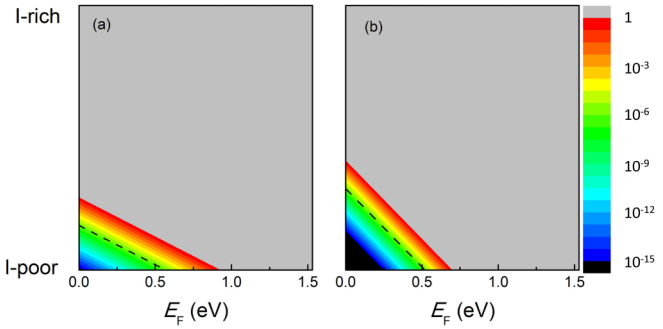

FIG. 6. Dependence of the maximum lifetime (unit: seconds) of the (a) hole and (b) electron carriers on the Fermi energy and the growth conditions (from I-poor to I-rich). The black areas have lifetimes shorter than 1 fs, and the gray areas have lifetimes longer than 1 s. The black dashed lines divide the areas with the lifetimes longer and shorter than 1 μs. The ranges of the y axis (from I-rich to I-poor) and the whole figure are quantitatively determined based on the *ab initio* calculations, and a detailed description is given in Sec. IV of the Supplemental Material [35].

Previous experimental measurements showed that the carrier lifetime in single-crystal $CH_3NH_3PbI_3$ is around 1 μs [11–13]. According to our calculated carrier-capture rate, we can estimate that the concentration of Pb_I should be lower than $N_D = \frac{1}{B_h \tau} = 2.4 \times 10^{12}\,\mathrm{cm}^{-3}$ in n-type $CH_3NH_3PbI_3$ and lower than $3.6 \times 10^{14}\,\mathrm{cm}^{-3}$ in p-type $CH_3NH_3PbI_3$ in order to obtain such a long carrier lifetime. On the right side of the black dashed lines in Fig. 6, we show the growth conditions and Fermi energy range in which the concentration of Pb_I can be so low that the maximum carrier lifetime can be longer than 1 μs in single-crystal $CH_3NH_3PbI_3$. Obviously the carrier lifetime is longer than 1 μs in most of the area of Fig. 6, which explains why a long carrier lifetime was observed experimentally by several different groups. It should be noted that the carrier lifetime is not long in all $CH_3NH_3PbI_3$ single crystals. Our calculation showed that the electron lifetime is very short in p-type and I-poor $CH_3NH_3PbI_3$, so we call for a future experimental measurement in p-type and I-poor samples which will show a clear dependence of the carrier lifetime on the growth conditions and the doping level.

Due to the short carrier lifetime, p-type doping should be avoided if we want to fabricate a high-efficiency solar cell using the I-poor $CH_3NH_3PbI_3$ as the light-absorbing material. In contrast, there is no such limit for I-rich $CH_3NH_3PbI_3$. Previously it was believed that the point defects were benign in the $CH_3NH_3PbI_3$ perovskites [14,15,49], but our quantitative calculation of the carrier-capture rates of Pb_I demonstrates the necessity of defect control through both the growth conditions and the doping level.

IV. CONCLUSIONS

We have implemented a new algorithm in the first-principles simulation package QUANTUM ESPRESSO to accelerate the expensive el-ph coupling calculation so that we predict the carrier-capture rate of point defects in the organic-inorganic hybrid perovskites. Using the method and the static coupling formalism, we studied the nonradiative recombination induced by Pb_I antisite in $CH_3NH_3PbI_3$. The calculated carrier-capture rates and cross sections are relatively large for both the electron and the hole carriers, which is attributed mainly to the heavy atoms and soft phonon modes in the Pb-I lattice. The increased thermal energy after the nonradiative recombination is stored mainly by the phonons in the soft Pb-I lattice, whereas the contribution of the organic CH_3NH_3 group is negligible. Our results show definitely that: (i) the Pb_I antisite acts as an effective recombination center in p-type $CH_3NH_3PbI_3$ grown under I-poor conditions and is detrimental to the photovoltaic performance; (ii) in order to achieve a high PCE, I-poor conditions and p-type doping should be avoided. Using this method we can predict the influence of various defects on the photovoltaic performance more accurately and guide the future development of high PCE solar cells through defect control.

ACKNOWLEDGMENTS

The authors would like to thank Dr. L.-W. Wang, Dr. L. Shi, and Dr. S. de Gironcoli for their help on the numerical algorithms and Dr. J.-H. Yang and Dr. S.-H. Wei for their inspiring discussion. This work was supported by the Special Funds for Major State Basic Research, National Science Foundation of China (NSFC) and the Supercomputer Center of Fudan University. S.C. was supported by NSFC under Grant No. 61574059, the Shu-Guang Program (China) (Program No. 15SG20), and the Computer Center of ECNU.

[1] T. M. Brenner, D. A. Egger, L. Kronik, G. Hodes, and D. Cahen, Nat. Rev. Mater. **1**, 15007 (2016).
[2] http://www.nrel.gov/pv/assets/images/efficiency_chart.jpg
[3] A. Kojima, K. Teshima, Y. Shirai, and T. Miyasaka, J. Am. Chem. Soc. **131**, 6050 (2009).
[4] J. Burschka, N. Pellet, S.-J. Moon, R. Humphry-Baker, P. Gao, M. K. Nazeeruddin, and M. Grätzel, Nature (London) **499**, 316 (2013).
[5] M. Liu, M. B. Johnston, and H. J. Snaith, Nature (London) **501**, 395 (2013).
[6] H. Zhou *et al.*, Science **345**, 542 (2014).
[7] N. J. Jeon, H. G. Lee, Y. C. Kim, J. Seo, J. H. Noh, J. Lee, and S. I. Seok, J. Am. Chem. Soc. **136**, 7837 (2014).
[8] Q. Chen, H. Zhou, Z. Hong, S. Luo, H.-S. Duan, H.-H. Wang, Y. Liu, G. Li, and Y. Yang, J. Am. Chem. Soc. **136**, 622 (2014).
[9] P. Docampo, J. M. Ball, M. Darwich, G. E. Eperon, and H. J. Snaith, Nat. Commun. **4**, 2761 (2013).
[10] D. Liu and T. L. Kelly, Nat. Photonics **8**, 133 (2014).
[11] D. Shi *et al.*, Science **347**, 519 (2015).
[12] M. I. Saidaminov *et al.*, Nat. Commun. **6**, 7586 (2015).
[13] Q. Dong, Y. Fang, Y. Shao, P. Mulligan, J. Qiu, L. Cao, and J. Huang, Science **347**, 967 (2015).

[14] W.-J. Yin, T. Shi, and Y. Yan, Appl. Phys. Lett. **104**, 063903 (2014).
[15] J. Kim, S.-H. Lee, J. H. Lee, and K.-H. Hong, J. Phys. Chem. Lett. **5**, 1312 (2014).
[16] W. J. Yin, T. Shi, and Y. Yan, Adv. Mater. **26**, 4653 (2014).
[17] M. H. Du, J. Mater. Chem. A **2**, 9091 (2014).
[18] A. Buin, P. Pietsch, J. Xu, O. Voznyy, A. H. Ip, R. Comin, and E. H. Sargent, Nano Lett. **14**, 6281 (2014).
[19] A. Buin, R. Comin, J. Xu, A. H. Ip, and E. H. Sargent, Chem. Mater. **27**, 4405 (2015).
[20] T. Tsuchiya, Appl. Phys. Express **4**, 094104 (2011).
[21] M. A. Reshchikov, A. A. Kvasov, M. F. Bishop, T. McMullen, A. Usikov, V. Soukhoveev, and V. A. Dmitriev, Phys. Rev. B **84**, 075212 (2011).
[22] S. Juršėnas, S. Miasojedovas, G. Kurilčik, A. Žukauskas, and P. R. Hageman, Appl. Phys. Lett. **83**, 66 (2003).
[23] L. Shi and L.-W. Wang, Phys. Rev. Lett. **109**, 245501 (2012).
[24] L. Shi, K. Xu, and L.-W. Wang, Phys. Rev. B **91**, 205315 (2015).
[25] G. D. Barmparis, Y. S. Puzyrev, X.-G. Zhang, and S. T. Pantelides, Phys. Rev. B **92**, 214111 (2015).
[26] A. Alkauskas, Q. Yan, and C. G. Van de Walle, Phys. Rev. B **90**, 075202 (2014).
[27] A. Alkauskas, C. E. Dreyer, J. L. Lyons, and C. G. Van de Walle, Phys. Rev. B **93**, 201304(R) (2016).
[28] J.-H. Yang, L. Shi, L.-W. Wang, and S.-H. Wei, Sci. Rep. **6**, 21712 (2016).
[29] M. L. Agiorgousis, Y.-Y. Sun, H. Zeng, and S. Zhang, J. Am. Chem. Soc. **136**, 14570 (2014).
[30] P. Giannozzi *et al.*, J. Phys.: Condens. Matter **21**, 395502 (2009).
[31] F. J. A. Ferrer, J. Cerezo, J. Soto, R. Improta, and F. Santoro, Comput. Theor. Chem. **1040–1041**, 328 (2014).
[32] A. Baiardi, J. Bloino, and V. Barone, J. Chem. Theory Comput. **9**, 4097 (2013).
[33] R. Borrelli, A. Capobianco, and A. Peluso, J. Phys. Chem. A **116**, 9934 (2012).
[34] P. Umari, E. Mosconi, and F. De Angelis, Sci. Rep. **4**, 4467 (2014).
[35] See Supplemental Material at http://link.aps.org/supplemental/10.1103/PhysRevB.96.104103 for the benchmark test and more calculation details.
[36] M. C. Payne, M. P. Teter, D. C. Allan, T. Arias, and J. Joannopoulos, Rev. Mod. Phys. **64**, 1045 (1992).
[37] P. Giannozzi, F. De Angelis, and R. Car, J. Chem. Phys. **120**, 5903 (2004).
[38] W. Shockley and W. T. Read, Phys. Rev. **87**, 835 (1952).
[39] R. N. Hall, Phys. Rev. **87**, 387 (1952).
[40] G. Bemski, Phys. Rev. **111**, 1515 (1958).
[41] A. M. Stoneham, *Theory of Defects in Solids: Electronic Structure of Defects in Insulators and Semiconductors* (Oxford University Press, Oxford, 2001).
[42] C. Henry and D. V. Lang, Phys. Rev. B **15**, 989 (1977).
[43] V. L. Bonch-Bruevich and E. G. Landsberg, Phys. Status Solidi B **29**, 9 (1968).
[44] K. Huang, Prog. Phys. **1**, 31 (1981).
[45] K. F. Freed and J. Jortner, J. Chem. Phys. **52**, 6272 (1970).
[46] R. Kubo and Y. Toyozawa, Prog. Theor. Phys. **13**, 160 (1955).
[47] K. Huang and A. Rhys, Proc. R. Soc. London, Ser. A **204**, 406 (1950).
[48] C. Deng, Y. Niu, Q. Peng, A. Qin, Z. Shuai, and B. Z. Tang, J. Chem. Phys. **135**, 014304 (2011).
[49] W.-J. Yin, J.-H. Yang, J. Kang, Y. Yan, and S.-H. Wei, J. Mater. Chem. A **3**, 8926 (2015).